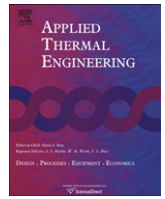




Contents lists available at ScienceDirect

# Applied Thermal Engineering

journal homepage: [www.elsevier.com/locate/apthermeng](http://www.elsevier.com/locate/apthermeng)

## Pyroelectric energy converter using co-polymer P(VDF-TrFE) and Olsen cycle for waste heat energy harvesting

Hiep Nguyen, Ashcon Navid, Laurent Pilon\*

University of California, Los Angeles Henry Samueli School of Engineering and Applied Science, Mechanical and Aerospace Engineering Department, Los Angeles, CA 90095-1597, USA

### ARTICLE INFO

#### Article history:

Received 11 January 2010

Accepted 18 May 2010

Available online 31 May 2010

#### Keywords:

Pyroelectricity

Direct energy conversion

Waste heat harvesting

Ferroelectric

Olsen cycle

### ABSTRACT

This study was concerned with designing, building, and testing a pyroelectric energy converter to directly convert waste heat into electricity. The pyroelectric effect refers to the flow of charges to or from the surface of a material upon heating or cooling. The device consisted of a teflon cylindrical chamber with a piston oscillating vertically and driving a working fluid back and forth between a heat source and a cold heat exchanger. The Olsen cycle was performed on co-polymer 60/40 poly(vinylidene fluoride–trifluoroethylene) [P(VDF-TrFE)] thin films sandwiched between metallic electrodes. Their temperature oscillation, charge, voltage and the overall heat input and output were measured experimentally. Then, the electrical power generated and the energy efficiency were computed. The effects of channel width, frequency, and stroke length on temperature swing, heat input, as well as energy and power densities were investigated. Reducing the channel width and increasing the stroke length had the largest effect on device performance. A maximum energy density of 130 J/l was achieved at 0.061 Hz frequency with temperature oscillating between 69.3 and 87.6 °C. Furthermore, a maximum power density of 10.7 W/l was obtained at 0.12 Hz between 70.5 and 85.3 °C. In both cases, the low and high electric fields in the Olsen cycle were 202 and 739 kV/cm. To the best of our knowledge, this is the largest energy density achieved by any pyroelectric energy converter using P(VDF-TrFE). It also matches performances reported in the literature for more expensive lead zirconate stannate titanate (PZST) ceramic films operated at higher temperatures.

© 2010 Elsevier Ltd. All rights reserved.

### 1. Introduction

In the last decades, direct energy conversion devices for medium and low grades waste heat have received significant attention due to the necessity to develop more energy efficient engineering systems. In fact, in 2002 more than 50% of the net primary energy resource consuming in the U.S. was lost mainly in the form of waste heat [1]. To date, the effort has focused on thermoelectric generators based on the Seebeck effect that results in the creation of an electromagnetic force (emf) in the presence of a steady-state temperature difference between two junctions of dissimilar metals or semiconductors. It has been reported that commercial thermoelectric generators have efficiencies that are “typically around 5%” [2]. Higher efficiencies have been achieved with expensive nanostructured thermoelectric materials after 50 years of research efforts [3]. Stirling engines can also operate at low temperatures to convert waste heat into mechanical energy but

their performance is hindered by heat losses and an additional step is required to convert mechanical energy into electricity by means of an electrical generator or dynamo. Alternatively, organic Rankine cycles use organic working fluids such as refrigerants and hydrocarbons instead of water to harvest waste heat at temperatures up to 200–300 °C [4].

Pyroelectric energy conversion offers a novel and direct way to convert waste heat into electricity by alternatively heating and cooling a pyroelectric material resulting in electricity generation [5–10]. It makes use of the pyroelectric effect to create a flow of charge to or from the surface of a pyroelectric material as a result of heating or cooling [11]. The fact that very small changes in temperature (~mK) can produce a pyroelectric current on the order of nA or pA [11] has been used extensively in infrared detection for imaging and motion sensing as well as for thermometry applications [12]. The use of pyroelectric materials to harvest waste heat has been explored both experimentally and theoretically. While early theoretical studies predicted low efficiencies [13,14], experimental studies [5,7,8,10,15–18] have achieved significantly better results. Overall, however, little efforts have been dedicated to developing pyroelectric energy conversion.

\* Corresponding author. Tel.: +1 (310) 206 5598; fax: +1 (310) 206 4830.  
E-mail address: [pilon@seas.ucla.edu](mailto:pilon@seas.ucla.edu) (L. Pilon).

Nomenclature	
$A$	surface area of the PE, $m^2$
$b$	film thickness, $m$
$C_1$	capacitance, $F$
$c_p$	specific heat, $J/kg \cdot K$
$D_{PE}$	electric displacement of the PE, $C/m^2$
$D_h$	hydraulic diameter, $m$
$E_{PE}$	electric field across the PE, $V/cm$
$E_L, E_H$	low and high electric fields, $V/m$
$F_p$	power factor, Eq. (9)
$f$	frequency, $1/s$
$h_\omega$	convective heat transfer coefficient for oscillating flow, $W/m^2 \cdot K$
$I_L$	leakage current, $A$
$I_p$	pyroelectric current, $A$
$I_{rms}$	Kapton electrical heater current, $A$
$k_f$	fluid thermal conductivity, $W/m \cdot K$
$L$	channel length, $m$
$l_0$	amplitude of fluid flow displacement, $m$
$\dot{m}_c$	cold heat exchanger mass flow rate, $kg/s$
$n_{PE}$	number of pyroelectric elements
$N_D$	energy density, $J/l$
$Nu_\omega$	Nusselt number for oscillating flow
$p_c$	pyroelectric coefficient, $C/m^2 \cdot K$
$P_D$	power density, $W/l$
$Pr_f$	Prandtl number, Eq. (16)
$P_S$	spontaneous polarization, $C/m^2$
$q_{PE}$	charges on the PE electrodes, $C$
$\dot{Q}_{in}$	heat transfer rate into the device, $W$
$\dot{Q}_{losses}$	heat losses, $W$
$\dot{Q}_{out}$	heat transfer rate to the cold heat exchanger, $W$
$r_{PE}$	electrical resistivity of the PE, $\Omega \cdot m$
$R_1, R_2$	output and input current resistances, $\Omega$
$R_L$	load resistance, $\Omega$
$Re_\omega$	Reynolds number for oscillating flow, Eq. (16)
$S$	piston stroke length, $m$
$St, St_L$	Strouhal numbers, Eq. (15)
$t$	time, $s$
$T_i$	temperature at location $i$ , $^\circ C$ or $K$
$\bar{T}_i$	mean temperature at location $i$ , $^\circ C$ or $K$
$T_{c, i}, T_{c, o}$	cold heat exchanger inlet and outlet temperatures, $^\circ C$
$T_{Curie, \downarrow}$	Curie temperature from para- to ferroelectric phase change, $^\circ C$
$T_{Curie, \uparrow}$	Curie temperature from ferro- to paraelectric phase change, $^\circ C$
$\Delta T_i$	temperature swing at location $i$ , $^\circ C$
$u_0$	amplitude of velocity oscillation, $m/s$
$V_1, V_2$	measured voltage across $C_1$ and $R_2$ , $V$
$V_L, V_H$	low and high voltage, $V$
$V_m$	measured voltage across resistor $R_D$ , $V$
$V_{PE}$	voltage across the PEs, $V$
$V_{rms}$	Kapton electrical heater voltage, $V$
$\forall$	volume, $m^3$
$W_E$	electrical work output, $J$
$\dot{W}_{cycle}$	net electrical power generated over a cycle, $W$
$\dot{W}_E$	generated electrical power, $W$
$\dot{W}_p$	piston pumping power, $W$
$z$	vertical coordinate in $(x,z)$ coordinate system
<b>Greek symbols</b>	
$\alpha_f$	fluid thermal diffusivity, $m^2/s$
$\eta$	thermodynamic efficiency, %
$\eta_{Carnot}$	Carnot efficiency, %
$\omega$	piston angular velocity, $rad/s$
$\nu_f$	fluid kinematic viscosity, $cst$
$\rho$	density, $kg/m^3$
$\tau$	period of oscillation ( $=1/f$ ), $s$
$\tau_t$	thermal time constant, $s$
<b>Subscripts</b>	
$c$	refers to cold fluid
$H, L$	refers to high and low values
$PE$	refers to pyroelectric element
min, max	refers to minimum and maximum values

The objectives of the present study are: (1) to design and assemble a fully instrumented pyroelectric energy converter performing the Olsen cycle on co-polymer poly(vinylidene fluoride–trifluoroethylene) [P(VDF-TrFE)], (2) to experimentally measure temporal temperature and pressure evolutions at various locations throughout the device, and (3) to improve the energy and power densities of the pyroelectric energy converter built by Olsen and co-workers [5,10].

## 2. Current state of knowledge

### 2.1. Material considerations

Pyroelectric materials possess a spontaneous polarization in the absence of an applied electric field. The spontaneous polarization is strongly dependent of temperature due to the pyroelectric material's crystallographic structure [11]. The displacement of the atoms from their equilibrium positions upon heating and cooling results in the pyroelectric effect. The electric current  $I_p$  generated by pyroelectric materials is given by  $I_p = Ap_c dT/dt$  where  $A$  is the surface area of the pyroelectric material,  $p_c$  is the pyroelectric coefficient, and  $dT/dt$  is the heating or cooling rate [15]. Note that this is not valid for large temperature changes due to non-linear material behavior [19].

Moreover, ferroelectricity is the ability of a material to have a spontaneous polarization  $-P_S$  which can be reversed to  $+P_S$  by applying an electric field. Ferroelectric materials have a history dependent response to an applied electric field which results in a hysteresis loop. The electric displacement in the absence of an applied electric field is called the spontaneous polarization  $P_S$  while the electric field that is needed to reach zero displacement is called the coercive field. The maximum electric field that the material can withstand without being conductive is called the electric breakdown field or dielectric strength while the maximum electric displacement that can be achieved by the cycle is called the displacement saturation [20]. Some pyroelectric materials such as P(VDF-TrFE) are also ferroelectric.

Paraelectricity is the ability of a material with no spontaneous polarization to become polarized under an applied electric field [21]. Paraelectricity takes place in crystal structures where the electric dipole moments are unaligned, but have the potential to be aligned when subjected to an external electric field.

Curie phase transition corresponds to the material phase change from ferroelectric to paraelectric or vice versa, upon heating or cooling, respectively. The Curie temperature at which the transition from ferro- to paraelectric occurs is denoted by  $T_{Curie, \uparrow}$  and the Curie temperature at which the material transitions from para- to

ferroelectric is denoted by  $T_{\text{Curie}, \downarrow}$ . Note that the phase transition from ferroelectric to paraelectric is accompanied by a large discharge of electrical energy. It is, thus, advantageous to heat and cool ferroelectric materials across  $T_{\text{Curie}, \uparrow}$  [22].

## 2.2. Polymeric pyroelectric materials

PVDF and its co-polymer P(VDF-TrFE) have received considerable attention due to their large pyroelectric coefficient used in biomedical and industrial applications [20]. Unlike PVDF, co-polymer P(VDF-TrFE) crystallizes into the ferroelectric  $\beta$ -phase in absence of external stresses [23]. Thus, re-poling P(VDF-TrFE) requires only cooling below  $T_{\text{Curie}, \downarrow}$  and under electric poling. On the contrary, re-poling PVDF requires not only electric poling but also mechanical deformation.

Parameters that affect  $T_{\text{Curie}, \uparrow}$  and  $T_{\text{Curie}, \downarrow}$  of P(VDF-TrFE) include VDF/TrFE ratio, magnitude of the applied electric field, and polymer processing techniques [24]. It has been established that  $T_{\text{Curie}, \uparrow}$  increases as VDF/TrFE ratio increases due to an increase in the disorder of the co-polymer domains [20]. In addition,  $T_{\text{Curie}, \uparrow}$  was shown to increase with the applied electric field [25]. For example,  $T_{\text{Curie}, \uparrow}$  for 60/40 P(VDF-TrFE) is approximately 66 °C at zero field [26] and increases to 120 °C when the field is 527 kV/cm [25].

## 2.3. Pyroelectric energy conversion

### 2.3.1. Olsen cycle

The so-called Olsen cycle is the electric analog of the Ericsson heat engine in the charge–voltage diagram ( $q$ - $V$ ) as opposed to the pressure-volume ( $p$ - $v$ ) diagram. The cycle was developed by Olsen and co-workers between 1978 and 1985 [10,11,15,20,22,23,27,28]. Fig. 1 shows the  $q$ - $V$  diagram of a typical pyroelectric element (PE) where the Olsen cycle is represented by the 1–2–3–4 loop. A pyroelectric element consists of a pyroelectric thin film and its metallic electrodes deposited on both faces. The Olsen cycle begins by charging the PE at low temperature  $T_L$  by increasing the voltage from  $V_L$  to  $V_H$  (process 1–2). Next, the PE is discharged by heating the element from  $T_L$  to  $T_H$  at constant voltage  $V_H$  where ideally  $T_H > T_{\text{Curie}, \uparrow}$  (process 2–3). The material is further discharged by reducing the voltage from  $V_H$  to  $V_L$  at constant temperature  $T_H$  (process 3–4). Finally, the PE is recharged by cooling it from  $T_H$  to  $T_L < T_{\text{Curie}, \downarrow}$  at constant voltage  $V_L$  (process 4–1) [23]. The shaded

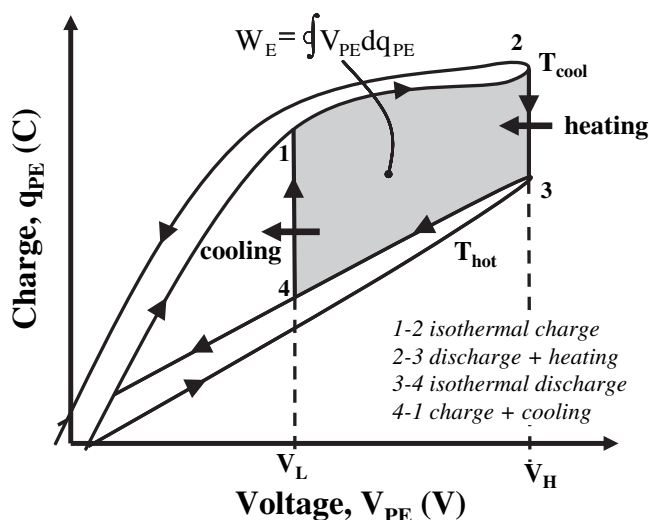


Fig. 1. Charge versus voltage for a typical pyroelectric material at different temperatures. The Olsen power cycle is represented by the area between 1–2–3–4.

area in Fig. 1 corresponds to the electrical work output  $W_E$  expressed in J/l and given by,

$$W_E = \oint V_{PE} dq_{PE} \quad (1)$$

Note that heating and cooling the pyroelectric element above and below the Curie temperatures are not required during the cycle, but doing so could result in a larger electrical energy production as previously discussed.

### 2.3.2. Pyroelectric energy converters based on Olsen cycle

To the best of our knowledge, only five prototypical pyroelectric converters have been built to date. Table 1 summarizes the pyroelectric material and the working fluid used as well as the optimum operating frequency and performance reported in previous studies. For example, Olsen *et al.* [5] assembled a regenerative and multi-stage device using lead zirconate stannate titanate (PZST) thin films with various compositions in which  $\text{Ti}^{4+}$  was substituted by  $\text{Sn}^{4+}$ . Heat input into the device was provided by a resistive stainless steel heating band while cooling was achieved via a copper cooling coil. A ceramic stack consisting of 100 layers of alumina sheets separated by microchannels filled with working fluid was placed vertically between the heat source and the cold heat exchanger. A piston oscillated the working fluid back and forth between heat source and cold heat exchanger at 185 and 145 °C, respectively. In addition, four PZST pyroelectric elements were placed in thermal contact with the working fluid. The low voltage  $V_L$  applied to the PEs was kept constant at 100 V or an electric field of 4 kV/cm while the high voltage  $V_H$  was varied between 100 and 700 V (28 kV/cm). The maximum output power density achieved was 33 W/l of PZST at 0.26 Hz for  $V_H$  equal to 700 V corresponding to an efficiency of 0.56% [5].

Although PZST has attractive pyroelectric properties for power generation applications, its cost, estimated as ~\$10,000/Watt, makes its use impractical [10]. Therefore, Olsen *et al.* [10] proposed to use inexpensive 73/27 P(VDF-TrFE) thin films 30–70  $\mu\text{m}$  in thickness. Instead of using a ceramic stack, the PEs were embedded into a spiral stack constructed by alternate layers of plastic sheets and nylon separator screens [10]. The low and high electric field were 230 and 530 kV/cm and the device was able to generate a maximum energy density of 30 J/l [10].

### 2.3.3. Performance of pyroelectric energy converters

In order to assess the performance of the pyroelectric converter, the thermodynamic energy efficiency of the system over a cycle is defined as [29],

$$\eta = \frac{\dot{W}_{\text{cycle}}}{\dot{Q}_{\text{in}}} = \frac{n_{PE} \dot{W}_E - \dot{W}_p}{\dot{Q}_{\text{in}}} \quad (2)$$

where  $\dot{Q}_{\text{in}}$  (in W) is the heat transfer rate provided to the converter,  $\dot{W}_{\text{cycle}}$  (in W) is the net power produced by the device, and  $n_{PE}$  is the number of pyroelectric elements used for power generation. The electrical power produced by a single PE and the power consumed for pumping the working fluid are denoted by  $\dot{W}_E$  and  $\dot{W}_p$ , respectively.

### 2.3.4. Leakage current

A pyroelectric element can be represented by a current generator, a capacitor, and a resistor in parallel. The direction of generated current reverses upon heating and cooling. Ideally, the resistance of the pyroelectric element should be infinite which corresponds to zero leakage across the PE. In reality, however, the resistance is finite and decreases as the applied electric field and

**Table 1**  
Summary of design and performance of pyroelectric converters built to date.

Ref.	Material	Thickness	Fluid	$T_{\text{cold}}/T_{\text{hot}}$ (°C)	f (Hz)	Electrodes	$V_L/V_H$ (V)	Electrical output	$\eta$ (%)
[5]	PZST	250 $\mu\text{m}$ flat stack	Silicone oil (50cst)	145/185	0.14	Ni (sputtered)	100/1100	1.37 W	1.05
[6]	PZST	250 $\mu\text{m}$ flat stack	Silicone oil (200cst)	146/159	0.14	Ni (sputtered)	0/700	100 J/l/cycle	N/A
[7]	PZST	250 $\mu\text{m}$ flat stack	Silicone oil (100cst)	145/178	0.128	Ni (sputtered)	300/800	130 J/l/cycle	0.42
[9]	PZST	250 $\mu\text{m}$ flat stack	Silicone oil (200cst)	110/170	0.04	Ag (fired-on)	0/700	0.36 J/l/cycle	N/A
[10]	P(VDF-TrFE) 73/27	30–70 $\mu\text{m}$ spiral stack	Silicone oil (200cst)	20/90	0.08–0.5	Al	200/550	30 J/l/cycle	N/A

temperature increase. As a result, a so-called leakage current denoted by  $I_L$  flows through the PE, thus, reducing the electrical energy produced [10,15,22,23]. Leakage current increases with increasing temperature and increasing voltage [25].

### 3. Experimental setup and procedures

A pyroelectric converter was designed and fabricated to directly convert thermal energy into electrical energy based on the Olsen cycle [10]. Fig. 2 shows a cross-section of the device along with a photograph. The device consisted of a thermal and an electrical sub-systems. The reader is referred to Ref.[30] for detailed description and discussion of the device and its operation.

#### 3.1. Thermal sub-system

The thermal sub-system consisted of five major parts, namely (i) the piston-cylinder assembly, (ii) the pyroelectric elements, (iii) the heating source, (iv) the cold heat exchanger, and (v) the working fluid. The piston oscillated the working fluid vertically between the heater located at the top of the device and the cold heat exchanger located at the bottom. Enclosure cylinders made of Teflon were used to guide the motion of the working fluid and acted also as thermal insulation and as a support on which parts were mounted. The cylinder had inner and outer diameters of 38.10 and 57.15 mm,

respectively. Two 3.20 mm diameter holes were drilled onto the part where they were offset from the center by 25 mm. Two 25 cm in length M3 threaded rods were inserted into these holes in order to hold the device together. Teflon was used for outer cylinders because of its low density and thermal conductivity which minimized the device's weight and heat losses. In fact, the density and thermal conductivity of Teflon at room temperature are 357 kg/m<sup>3</sup> and 0.25 W/mK, respectively. Teflon can also operate at temperature up to 260 °C [31]. Additionally, Teflon can be easily machined into the desired shapes unlike its ceramic counterparts such as Al<sub>2</sub>O<sub>3</sub> used by Olsen *et al.*[5]. Silicone gaskets were placed between enclosing cylinders to prevent the working fluid from leaking out to the environment.

#### 3.1.1. Piston-cylinder assembly

A piston and cylinder sleeve assembly of the Evolution 35GT2 two stroke gasoline engine were purchased from Evolution Engines [32]. The sleeve's inner diameter was 3.5 cm while its height was 6.4 cm. Both the sleeve and the piston were made of stainless steel and the fluid located within the cylinder sleeve was sealed from leaking via the piston ring mounted onto the piston head. A metal rod connected the piston to a flywheel powered by an electric motor model 2709K18 by McMaster-Carr. The piston stroke length was varied from 2.5 to 4.7 cm by changing the mounting radius of the connection between rod and the flywheel.

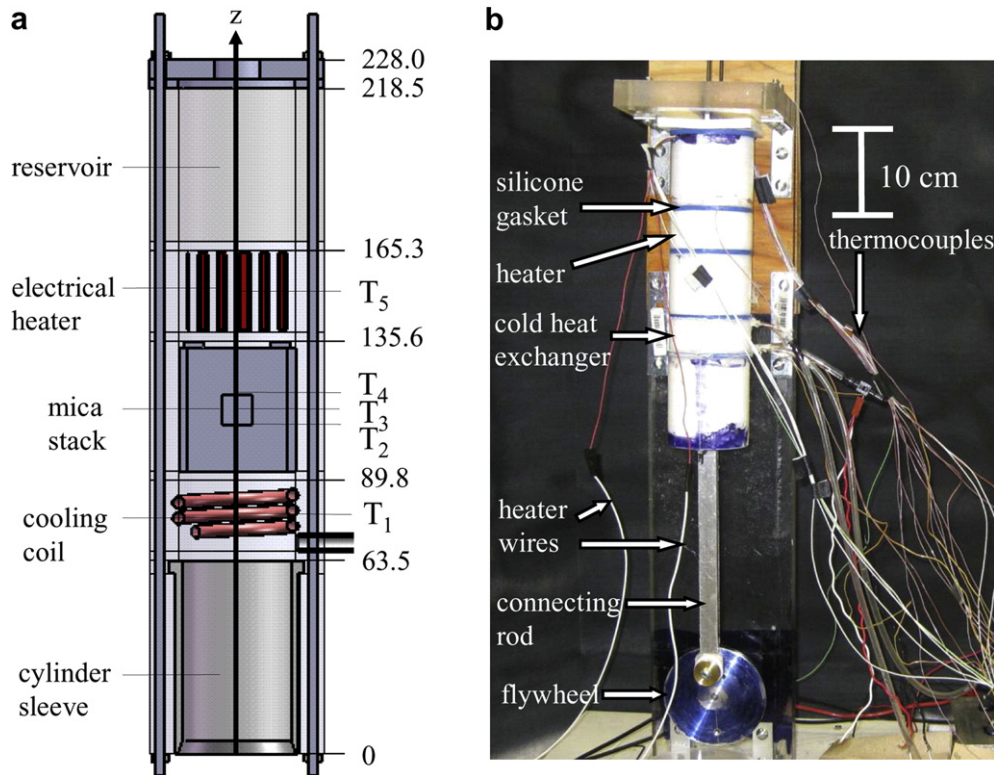


**Fig. 2.** (a) Schematic of the device cross-section and its corresponding components and (b) photograph of the actual device (all units are in millimeters).

### 3.1.2. Pyroelectric assembly and stack

Each pyroelectric element in the pyroelectric assembly was sandwiched between two mica plates to prevent it from moving horizontally and vertically. Fig. 3 shows the pyroelectric assembly and stack integration process. First, a 310  $\mu\text{m}$  thick mica plate was laid flat on a smooth surface where a 10 mm  $\times$  10 mm window was cut away in the plate's center using a knife. The length of the mica plates was 40.6 mm while their width varied from 20.8 to 38.1 mm so they could be stacked and fit into the Teflon cylinder.

Then, the PE was placed onto the plate and four pieces of 89  $\mu\text{m}$  thick Kapton tape were used to tape the edges of the PE to the mica plate. Afterwards, an electrical wire was connected to each electrode of the PE using 89  $\mu\text{m}$  thick copper tape. The wires were then guided outside of the device and connected to the electrical circuit described in Section 3.2. Next, an identical mica plate was pressed down on the edges of the PE. The two plates were bonded to one another via a thin layer of thermal epoxy at four corners. Two pieces of 3.18 mm wide and 330  $\mu\text{m}$  thick double sided Teflon tape were then adhered to the vertical edges of the mica plate where they bonded to another pyroelectric assembly to create a 330  $\mu\text{m}$  wide microchannel. Finally, the process was repeated in order to form a stack consisting of 38 pyroelectric elements. Note that the microchannel width can be made wider by using multiple layers of Teflon tape.

P(VDF-TrFE) was chosen as the pyroelectric material for power generation for its lower Curie temperature compared with typical ceramics (e.g., PZST) which makes it attractive for low grade waste heat harvesting applications. In addition, P(VDF-TrFE) has an electric breakdown field that is 25 times greater than that of PZST [10]. The material can be easily processed and costs ten times less than PZST [10]. Mica, on the other hand, was chosen as the PE supporting plates due to its high melting point, high dielectric strength, and its mechanical stiffness. Note that Teflon sheets of 381 and 508  $\mu\text{m}$  in thickness were also tested to support the PEs. However, the sheets

deformed upon the application of an electric field and/or heating, thus obstructing the microchannels and blocking the working fluid flow.

### 3.1.3. Heat source and cold heat exchanger

A flexible 50 W AC Kapton electrical heater was used as the heat source. It was taped to a thin copper sheet of dimensions 12.7 cm  $\times$  2.54 cm  $\times$  0.20 mm. The ensemble was subsequently bent to fit inside the Teflon cylinder and placed above the PE stack. The power input could be continuously increased up to a maximum of 50 W by increasing the voltage across the heater. On the other hand, the cold heat exchanger was made of a copper tube with inner and outer diameters equal to 1.59 mm and 3.18 mm (1/16" and 1/8"), respectively. The pipe was 34.3 cm long and was bent into a helical shape before being mounted onto the cold heat exchanger's outer cylinder. Cold water was fed into the coil via a DC electrical pump model W309-11 by Hargraves. The flow rate was adjusted in order to achieve the desired operating conditions.

### 3.1.4. Working fluid

Dow Corning 50 cst silicone oil was used as the working fluid by analogy with previous studies [5–10]. This oil is a dielectric fluid compatible with electronic components. Its relatively large viscosity ensures that the fluid flow was laminar in the microchannels. Furthermore, the oil's high dielectric strength of  $15.7 \times 10^6$  V/m at 25  $^\circ\text{C}$  [33] and its boiling point of 200  $^\circ\text{C}$  at atmospheric pressure make it attractive for pyroelectric power generation.

### 3.2. Electrical sub-system

Fig. 4 shows the electrical sub-system used in this study to both prepole the pyroelectric film and perform the Olsen cycle. The electrical sub-system controlled the voltage applied to the

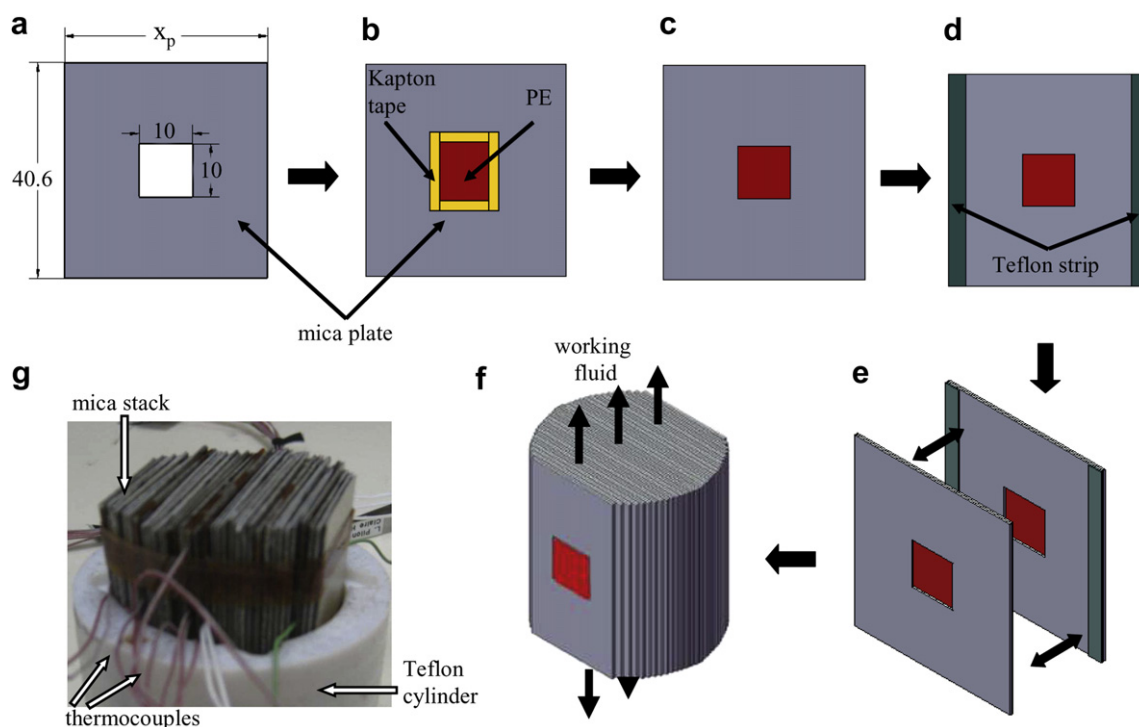


**Fig. 3.** Schematic of the pyroelectric stack assembling process showing (a) a mica plate with a 10  $\times$  10 mm window, (b) a mica plate with PE, (c) PE sandwiched between two mica plates, (d) pyroelectric assembly with Teflon strips, (e) mating of two mica plates, (f) entire PE stack, and (g) photograph of the actual stack (all dimensions are in millimeters).

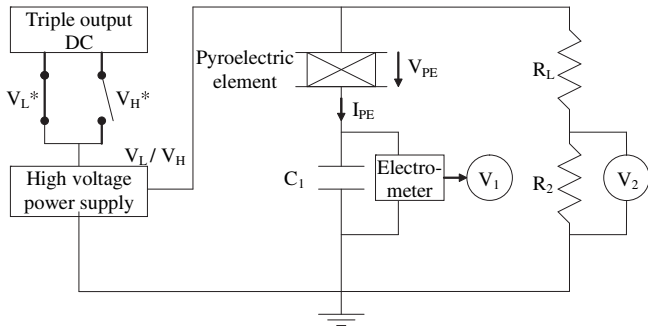


Fig. 4. Schematic of the electrical circuit used to prepoling and measure the electrical resistivity  $r_{PE}$  of the pyroelectric element and to perform the Olsen cycle.

pyroelectric element and imposed  $V_L$  or  $V_H$  at the appropriate time during the Olsen cycle. It also measured the power generated by the pyroelectric element by measuring the voltage  $V_{PE}$  and charge  $q_{PE}$ . The triple DC output power supply provided input voltages  $V_L^*$  and  $V_H^*$  to the high voltage power supply. Two rocker switches were connected to the high voltage power supply terminals to provide either voltage  $V_L^*$  or  $V_H^*$ . The latter converted the input voltage  $V_{L/H}^*$  to output voltage such that  $V_{L/H} = 250V_{L/H}^*$ . At all times, only one switch was permitted to be opened while the other was closed. The resistor  $R_L$  (7.80 M $\Omega$ ) acted as a voltage divider to scale down the voltage across the resistor  $R_2$  (21.8 k $\Omega$ ) in order to match the maximum voltage input of 10 V of the data acquisition system (DAQ). Voltage  $V_1$  across capacitor  $C_1$  (1.0  $\mu$ F) and voltage  $V_2$  across resistor  $R_2$  were measured via the DAQ and used to calculate the magnitude of the PE's electric displacement  $D_{PE}$  and electric field  $E_{PE}$ . The voltage  $V_1$  was measured through a custom built electrometer to minimize the discharge of capacitor  $C_1$  in the DAQ. The magnitude of the electric displacement  $D_{PE}$  was defined as,

$$D_{PE} = \frac{q_{PE}}{A} = \frac{C_1 V_1}{A} \quad (3)$$

where  $A$  is the surface area of the pyroelectric element. The magnitude of the electric field across the pyroelectric element was computed via Ohm's and Kirchhoff's laws such that,

$$E_{PE} = \frac{V_{PE}}{b} = \frac{V_2(1 + R_L/R_2) - V_1}{b} \quad (4)$$

where  $b$  is the pyroelectric film's thickness. Then, the D-E plot (equivalent to q-V plots) for the pyroelectric element undergoing the Olsen cycle can be generated.

### 3.3. Power generation analysis

#### 3.3.1. Resistivity

The pyroelectric element was prepoling and its resistivity was measured as a function of time before performing the Olsen cycle. The PE was held at a constant temperature of 85  $^{\circ}$ C while a constant voltage was applied across the PE. The leakage current  $I_L$  was expressed as,

$$I_L = C_1 \frac{dV_1}{dt} \quad (5)$$

where  $V_1$  is the registered voltage across capacitor  $C_1$  (Fig. 4). Moreover, the poling electric field applied across the PE computed from Eq. (4) was found to be 201 kV/cm.

Then, the film electrical resistivity, expressed in  $\Omega$ .m, was determined as,

$$r_{PE} = \frac{V_{PE}A}{I_L b} = \frac{E_{PE}A}{I_L} \quad (6)$$

#### 3.3.2. Power generation

Voltages  $V_1$  and  $V_2$  along with temperature  $T_{PE}$  were measured and recorded simultaneously as the Olsen cycle was performed. The energy density  $N_D$  of one cycle is represented by the enclosed area within the electric displacement versus electric field ( $D$ - $E$ ) curve and is given by,

$$N_D = \oint E_{PE} dD_{PE} = \frac{W_E}{V} \quad (7)$$

where the volume of the PE is  $V = Ab$ . In practice, the integral was estimated numerically using the trapezoid rule. The power density for a single pyroelectric element, denoted by  $P_D$ , is the power generated per liter of pyroelectric material. It is expressed as,

$$P_D = \frac{N_D}{\tau} = \frac{\dot{W}_E}{V} \quad (8)$$

where  $\tau$  is the period of a cycle and  $\dot{W}_E$  is the power generated by the PE.

### 3.4. Instrumentation

#### 3.4.1. Piston frequency measurements

A transmissive sensor model HOA 0866-N55 by Honeywell was used to measure the frequency of the oscillating piston. It consisted of an infrared emitting diode and a bipolar negative-positive-negative (NPN) silicon phototransistor.

#### 3.4.2. Temperature measurements

In order to determine the local temperatures within the device, type J thermocouples were securely mounted at various locations within the working fluid. Fig. 2 shows the location of the different thermocouples. The temperature  $T_1$  was measured at the center of the cold heat exchanger while  $T_2$ ,  $T_3$ , and  $T_4$  were the pyroelectric element' bottom, middle, and top temperatures, respectively. On the other hand, temperature  $T_5$  was measured using a type J thermocouple placed at the center of the heater cylinder. If one defines the  $z$ -axis along the axis of the device with origin  $z = 0$  set at its base, then, the temperatures  $T_1$ ,  $T_2$ ,  $T_3$ ,  $T_4$ , and  $T_5$  were measured at location  $z = 7.9$ , 10.8, 11.3, 11.8, and 15.2 cm, respectively. Moreover, the inlet and outlet temperatures of the cold heat exchanger, denoted by  $T_{c,i}$  and  $T_{c,o}$ , were measured with type K thermocouples placed within the feeding pipes. All thermocouples were connected to the DAQ for data recording and were calibrated for temperatures between 0 and 100  $^{\circ}$ C. Temperatures  $T_1$ ,  $T_2$ ,  $T_3$ ,  $T_4$ ,  $T_5$ ,  $T_{c,i}$ , and  $T_{c,o}$  were measured at a time interval of 0.05 s.

#### 3.4.3. Heat input and output measurements

A variac model 1010B by Staco Energy Products was used to control the voltage applied to the Kapton electrical heater. Its resistance and output voltage were adjusted to set the device heat input. The input power  $\dot{Q}_{in}$  was expressed as,

$$\dot{Q}_{in} = V_{rms} I_{rms} F_p \quad (9)$$

where  $F_p$  is the power factor and  $V_{rms}$  and  $I_{rms}$  are respectively the root mean-square voltage and current, simultaneously measured using a digital multimeter model 34401A by Agilent. The power factor was taken to be unity due to the fact that the heater's alternating current and voltage were in phase.

The mass flow rate  $\dot{m}_c$  from the DC electrical pump used to flow cold water through the cold heat exchanger was calibrated as a function of voltage [30]. The voltage across the pump was adjusted and recorded while the Olsen cycle was performed. The heat output removed by the cold heat exchanger was then computed as  $\dot{Q}_{out} = \dot{m}_c c_{p,c} (T_{c,o} - T_{c,i})$  where  $c_{p,c}$  is the specific heat of water at the mean temperature  $(T_{c,o} + T_{c,i})/2$ .

Finally, the overall energy balance of the device allows us to determine the performance of the cold heat exchanger and quantify the heat losses to the surroundings according to,

$$\dot{Q}_{losses} = \dot{Q}_{in} - n_{PE} \dot{W}_E - \dot{Q}_{out} \quad (10)$$

Where  $n_{PE}$  is the number of pyroelectric elements in the device.

## 4. Results and discussion

### 4.1. Preliminary tests

#### 4.1.1. Temperature measurements

Fig. 5 shows the temporal evolution of the fluid temperature near the cold heat exchanger  $T_1$  for piston frequency of 0.025 Hz, piston stroke length of 3.4 cm, channel width of 330  $\mu\text{m}$ , and heat input of 19 W. The minimum and maximum values of temperature  $T_1$  were 21.4 and 49.7  $^\circ\text{C}$ , respectively. Note that the temperature oscillations featured a frequency of 0.025 Hz in good agreement with the piston frequency measured independently. Similar results were obtained with the pressure at the bottom of the heat exchanger [30].

Moreover, Fig. 6 shows the temporal evolution of temperatures  $T_2$ ,  $T_3$ , and  $T_4$  along the pyroelectric assembly. The temperature swing  $\Delta T_i$  at location “i” is defined as,

$$\Delta T_i = T_{i,max} - T_{i,min} \quad (11)$$

where  $T_{i,max}$  and  $T_{i,min}$  are the maximum and minimum temperatures reached by  $T_i$  during one cycle. In addition, the arithmetic mean temperature  $\bar{T}_i$  at location “i” is defined as,

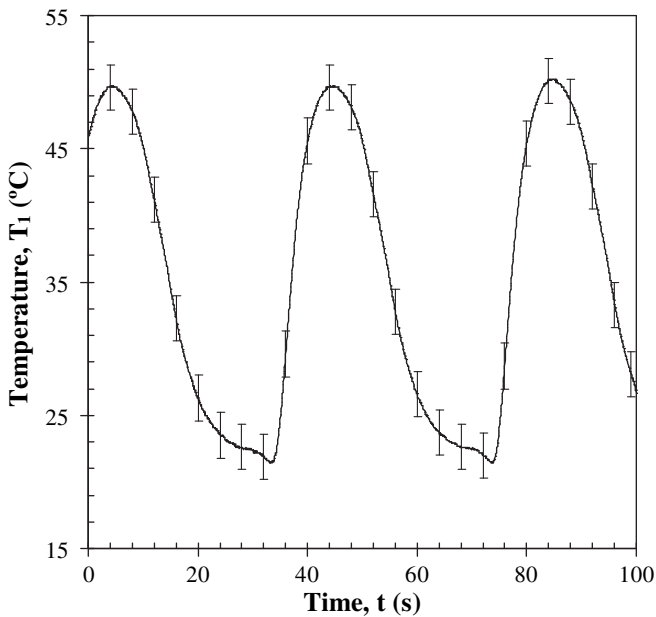


Fig. 5. Temporal temperature oscillation near the cold heat exchanger  $T_1$ . The piston oscillating frequency and stroke length, the stack channel width, and the heat input were constant and equal to 0.025 Hz, 3.4 cm, 330  $\mu\text{m}$ , and 19 W respectively.

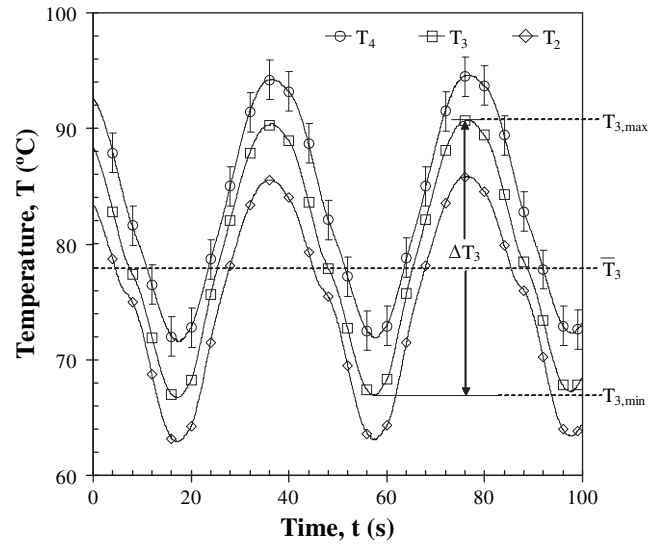


Fig. 6. Temporal evolutions of the working fluid temperatures at the bottom ( $T_2$ ), middle ( $T_3$ ), and top ( $T_4$ ) of the pyroelectric element. The piston oscillating frequency and stroke length, stack channel width, and the heat input were constant and equal to 0.025 Hz, 3.4 cm, 330  $\mu\text{m}$ , and 19 W, respectively.

$$\bar{T}_i = \frac{T_{i,max} + T_{i,min}}{2} \quad (12)$$

Fig. 6 indicates that  $T_3$ , measured in the middle of the PE, oscillated between 90.7 and 66.7 $^\circ\text{C}$ , resulting in a temperature swing  $\Delta T_3 = 24$   $^\circ\text{C}$ . Similarly,  $T_2$  oscillated between 85.9 and 62.9  $^\circ\text{C}$  while  $T_4$  oscillated between 94.6 and 71.6  $^\circ\text{C}$ , resulting in a temperature swing  $\Delta T_2 = \Delta T_4 = 23$   $^\circ\text{C}$ . As expected, the maximum temperature occurred when the piston was at the bottom of its stroke while the minimum temperature occurred when the piston was at the top of its stroke. Here also, the temperature oscillations had the same frequency as that of the piston. In the remaining of this study, the temperature  $T_3$  along with  $\bar{T}_3$  and  $\Delta T_3$  will be used as representative of the PE thermal response to oscillation of the working fluid.

#### 4.1.2. Power generation

A pyroelectric element made of P(VDF-TrFE) with VDF-TrFE weight ratio of 60/40 was prepoled in situ before performing the Olsen cycle. Fig. 7 plots the electrical resistivity  $r_{PE}$  of a 1 cm  $\times$  1 cm and 45.7  $\mu\text{m}$  thick P(VDF-TrFE) film measured as a function of time. The film was poled at  $E_{PE} = 201$  kV/cm and at  $T_3 = 85$   $^\circ\text{C}$  while the piston and the working fluid were at rest. The film resistivity  $r_{PE}$  increased rapidly during the first 10 min of poling. After 140 min, the resistivity was  $4.54 \times 10^{10}$   $\Omega\cdot\text{m}$  and did not change noticeably as poling continued. Thus, the poling process was stopped after 180 min. Similar poling procedure was followed for every runs reported in this study.

Once the poling process was completed, the Olsen cycle was performed on 45.7  $\mu\text{m}$  thick PEs. Fig. 8 shows the corresponding electrical displacement  $D_{PE}$  versus electric field  $E_{PE}$ . Here, the device had a stroke length of 4.7 cm and 330  $\mu\text{m}$  wide channels while operating at 0.061 Hz. The value of the low and high electric fields imposed in the Olsen cycle were  $E_L = 202$  kV/cm and  $E_H = 379$  kV/cm, respectively. The applied low electric field  $E_L$  was set at 202 kV/cm as suggested by Olsen *et al.*[10,25] in order to keep the film properly poled during process 4–1 of the Olsen cycle. The heat input provided by the heater was 30.9 W. The minimum and maximum temperatures measured at the center of the PE,  $T_{3,min}$  and  $T_{3,max}$ , were 66.4 and 83.0  $^\circ\text{C}$ , respectively corresponding to  $\Delta T_3 = 16.6$   $^\circ\text{C}$  and  $\bar{T}_3 = 74.7$   $^\circ\text{C}$ . The corresponding energy and

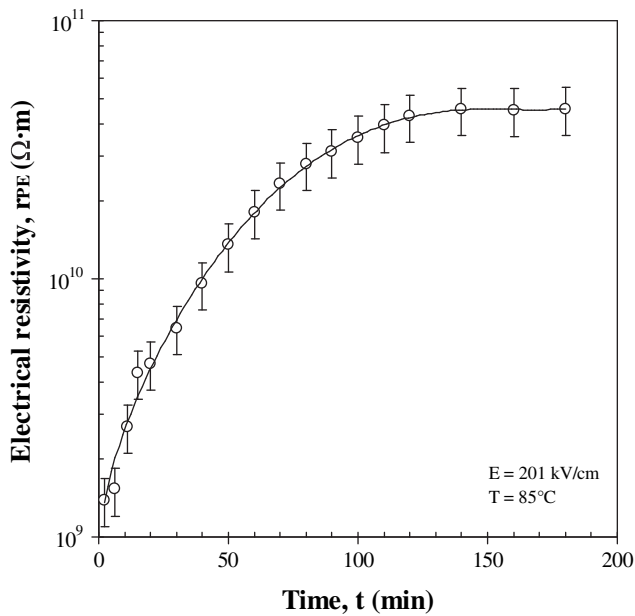


Fig. 7. Logarithmic of electrical resistivity of a 1 cm × 1 cm and 45.7 μm thick 60/40 P(VDF-TrFE) film as a function of time during poling at 201 kV/cm and  $T_3 = 85^\circ\text{C}$ .

power densities computed using Eqs. (7) and (8) were 130 J/l and 8.12 W/l of pyroelectric material, respectively.

4.1.3. Effect of temperature

Fig. 9 shows the energy density of a pyroelectric element as a function of arithmetic mean temperature at the center of the pyroelectric element  $\bar{T}_3$ . Here, the high field  $E_H$  was set to either 257 or 329 kV/cm. The channel width, stroke length, and frequency were 1 mm, 3.4 cm, and 0.025 Hz, respectively. In addition, the applied low electric field  $E_L$  was set at  $202 \pm 1$  kV/cm. The heat input provided by the electrical heater was adjusted in order to maintain  $\bar{T}_3$  at the desired temperature. Fig. 9 shows that a maximum energy density of 83 J/l of pyroelectric material was

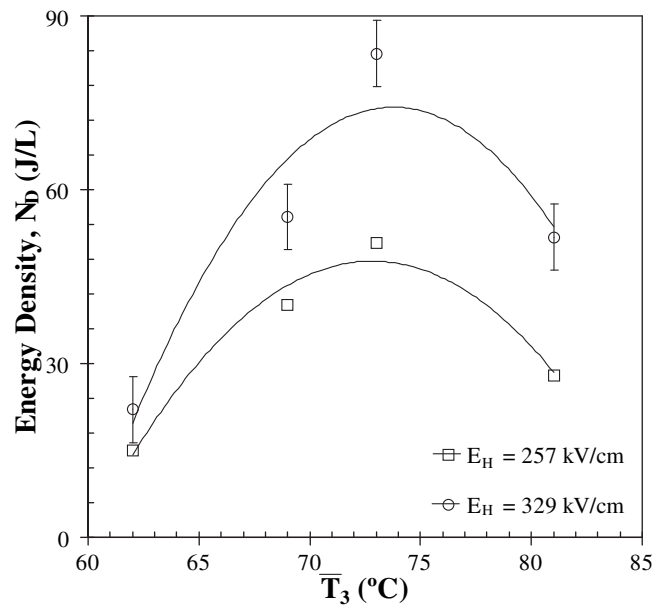


Fig. 9. Energy density as a function of  $\bar{T}_3$ . The channel width, piston stroke length and frequency, and low electric field were constant and equal to 1 mm, 3.4 cm, 0.025 Hz, and 202 kV/cm, respectively while the heat input by the electrical heater was adjusted to maintain  $\bar{T}_3$  at the desired temperature.

achieved when  $\bar{T}_3$  was about  $74 \pm 1^\circ\text{C}$  and  $E_H$  was 329 kV/cm. Exposing the center of the PE to a temperature  $\bar{T}_3$  larger than  $74^\circ\text{C}$  decreased the energy density of the pyroelectric element due to an increase in leakage current. On the other hand, exposing the center of the PE to a temperature  $\bar{T}_3$  smaller than  $74^\circ\text{C}$  resulted in smaller energy density due to a smaller temperature swing and to the fact that the PE may not undergo the ferro- to paraelectric phase transition. Indeed, the Curie temperature  $T_{\text{Curie}, \uparrow}$  for 60/40 P(VDF-TrFE) was reported to be equal to 90 and  $93^\circ\text{C}$  for 257 and 329 kV/cm electric field, respectively [25].

4.1.4. Preliminary conclusion

Preliminary tests showed that, as expected, the device's local temperatures and pressure oscillated sinusoidally at the same frequency as the piston. Moreover, electrical power was successfully generated by performing the Olsen cycle on 60/40 P(VDF-TrFE) films. The following sections report a systematic study of the effect of different parameters on the device's temperature swing, heat input, and electrical power generated. In all cases, the heat input was adjusted to maintain the arithmetic mean temperature at the center of the pyroelectric element  $\bar{T}_3$  at  $74 \pm 1^\circ\text{C}$  found to achieve the best compromise between large temperature swing and minimum leakage current.

4.2. Effect of channel width

Fig. 10 compares the temperature swing  $\Delta T_3$  at the center of the PE for channel width equal to 330 μm and 1 mm at frequency ranging from 0.025 to 0.16 Hz. The stroke length was equal to 3.4 cm. Fig. 10 indicates that the temperature swing  $\Delta T_3$  decreased with increasing frequency. This can be attributed to thermal inertia of both the working fluid and the pyroelectric element. As the frequency increased, there was less time for thermal energy to be exchanged between the heating band and the oscillating working fluid and between the working fluid and the pyroelectric elements. This limitation can be addressed by lowering the thermal time constant of the pyroelectric element defined as [34],

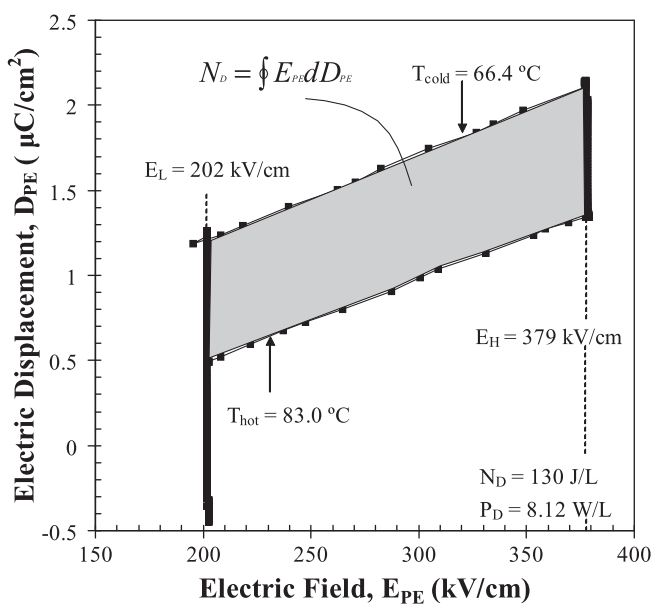
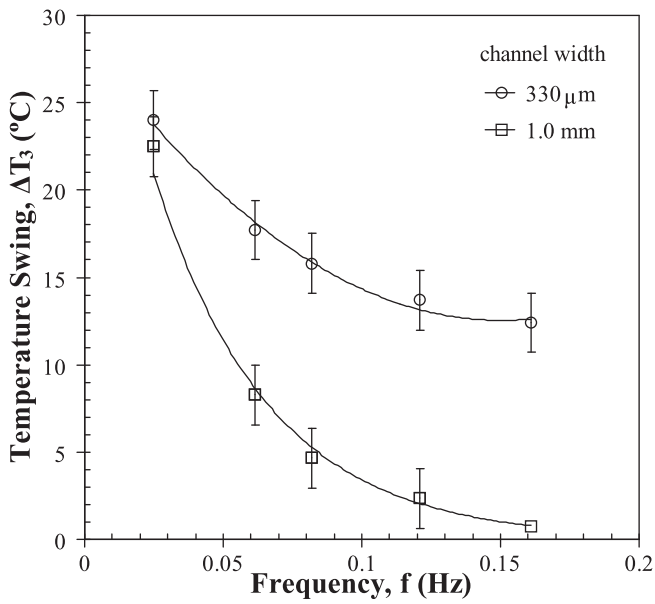


Fig. 8. Electric displacement versus electric field ( $D$ - $E$ ) for a 1 cm × 1 cm and 45.7 μm thick pyroelectric element. The piston stroke length, frequency, and channel width were 4.7 cm, 0.061 Hz, and 330 μm, respectively.



**Fig. 10.** Temperature swing  $\Delta T_3$  at the center of the pyroelectric element as a function of frequency measured for stack channel width equal to  $330 \mu\text{m}$  and  $1 \text{ mm}$ . The stroke length and the mean temperature  $\bar{T}_3$  were  $3.4 \text{ cm}$  and  $74 \pm 1 \text{ }^\circ\text{C}$ , respectively.

$$\tau_t = \frac{\rho_{PE} C_{p,PE} \nabla}{h_w A} \quad (13)$$

where  $h_w$  is the oscillatory flow convective heat transfer coefficient. The thermal time constant can be reduced by increasing  $h_w$  and the pyroelectric element surface area  $A$  and/or by decreasing the thickness of the pyroelectric element  $b = \nabla/A$ .

Moreover, Fig. 10 shows that a larger temperature swing was achieved with  $330 \mu\text{m}$  wide channels compared with  $1 \text{ mm}$  wide channels for the same  $\bar{T}_3$  value at all frequencies considered. Ozawa *et al.*[35] developed a correlation between the Strouhal, Reynolds, and Nusselt numbers for laminar oscillating flow in a circular channel given by,

$$Nu_\omega = \frac{h_\omega l_0}{k_f} = 0.92 St^{-0.2} St_L^{-0.26} Pr_f^{0.4} Re_\omega^{0.44} \quad (14)$$

where  $l_0$  and  $k_f$  are the amplitude of fluid displacement, and the thermal conductivity of the working fluid, respectively. The Strouhal numbers are denoted by  $St$  and  $St_L$  and defined as [35],

$$St = D_h/S \text{ and } St_L = L/S \quad (15)$$

Where  $D_h$  is the channel hydraulic diameter,  $S$  is the piston stroke length, and  $L$  is the channel length. In addition, the Reynolds and Prandtl numbers are denoted by  $Re_\omega$  and  $Pr_f$  and defined as [35],

$$Re_\omega = \frac{u_0 l_0}{\nu_f} = \frac{u_0^2}{\nu_f \omega} \text{ and } Pr_f = \frac{\nu_f}{\alpha_f} \quad (16)$$

where  $\nu_f$ ,  $\omega = 2\pi f$ ,  $u_0 = l_0 \omega$ , and  $\alpha_f$  are the fluid kinematic viscosity, piston angular frequency, amplitude of velocity oscillation, and fluid thermal diffusivity, respectively. As the channel width decreased, the hydraulic diameter decreased while the velocity of the working fluid increased thus, increasing the Strouhal  $St$  and Reynolds  $Re_\omega$  numbers. This, in turns, resulted in larger Nusselt number and heat transfer coefficient between the working fluid and the pyroelectric material, as suggested by Eq. [14] leading to larger temperature swing in the PE.

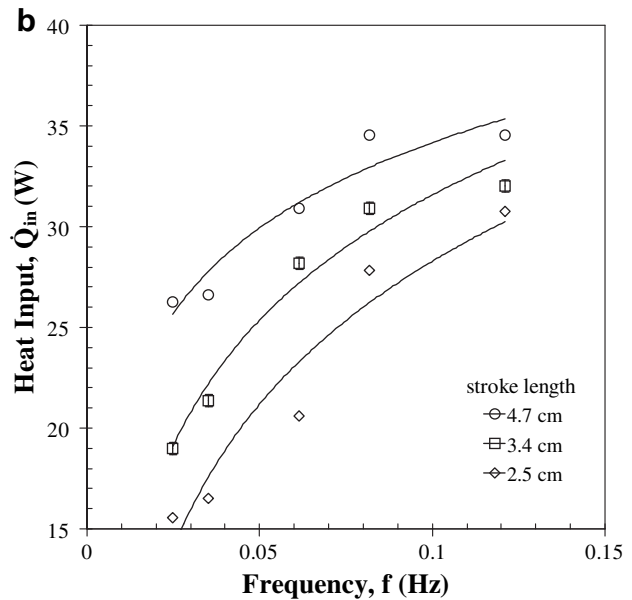
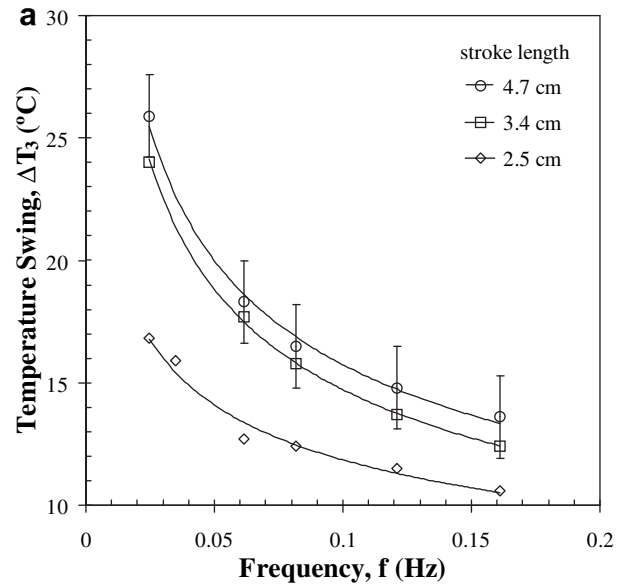


**Fig. 11.** (a) Temperature swing  $\Delta T_3$  at the center of the PE and (b) the associated heat input  $\dot{Q}_{in}$  as a function of frequency for piston stroke lengths of  $2.5$ ,  $3.4$ , and  $4.7 \text{ cm}$ . The channel width was  $330 \mu\text{m}$  and the mean temperature  $\bar{T}_3$  was  $74 \pm 1 \text{ }^\circ\text{C}$ .

#### 4.3. Effect of frequency and stroke length

Fig. 11a compares the temperature swing  $\Delta T_3$  at the center of the PE as a function of frequency for piston stroke length equal to  $2.5$ ,  $3.4$ , and  $4.7 \text{ cm}$ . It indicates that the temperature swing decreased as the frequency increased regardless of the stroke length, as previously discussed. Moreover, for a given frequency, the temperature swing increased as the stroke length increased from  $2.5$  to  $4.7 \text{ cm}$ . Increasing the stroke length to  $4.7 \text{ cm}$  allowed a fluid particle located at the heating band when the piston was at its highest position to carry the thermal energy down to the bottom of the PE as the piston reached its lowest position. As a result, a larger temperature swing was observed in the PE.

Fig. 11b shows the heat input  $\dot{Q}_{in}$  provided by the electrical heater to the working fluid as a function of piston frequency for stroke length equal to  $2.5$ ,  $3.4$ , and  $4.7 \text{ cm}$ . Data shown in Fig. 11b correspond to temperature swing  $\Delta T_3$  shown in Fig. 11a. It establishes that heat

input required to ensure the PE temperature  $\bar{T}_3 = 74 \pm 1 \text{ }^\circ\text{C}$  increased with frequency and stroke length. Indeed, as the frequency increased, the time during which thermal energy can be exchanged between the heating band and the working fluid decreased. This required a larger heat input to maintain  $\bar{T}_3$  at its prescribed value.

#### 4.4. Energy and power densities

##### 4.4.1. Effect of high electric field

Fig. 12 compares the energy density  $N_D$  as a function of high electric field  $E_H$  between 220 and 415 kV/cm for frequencies equal to 0.035, 0.061, and 0.12 Hz. The piston stroke length, channel width, and low electric field were 4.7 cm, 330  $\mu\text{m}$ , and 202 kV/cm, respectively. It shows that a maximum energy density of 130 J/l of pyroelectric material was obtained at 0.061 Hz with a high electric field  $E_H$  of 379 kV/cm. For  $E_H$  above 379 kV/cm, the energy density decreased due to increasing leakage current. On the other hand, applying  $E_H$  smaller than 379 kV/cm decreased the difference in electric field span ( $E_H - E_L$ ) and reduced the energy density as suggested by Eq. (7). Thus, the optimum value of  $E_H$  to maximize the energy density was found to be 379 kV/cm.

##### 4.4.2. Effect of frequency

Fig. 13 plots the maximum energy and power densities as a function of frequency. The piston stroke length, stack channel width, and arithmetic mean temperature at the center of the pyroelectric element  $\bar{T}_3$  were constant and equal to 4.7 cm, 330  $\mu\text{m}$ , and  $74 \pm 1 \text{ }^\circ\text{C}$ , respectively. The low and high electric fields were  $E_L = 202 \text{ kV/cm}$  and  $E_H = 379 \text{ kV/cm}$  as suggested by previous results. Even though the temperature swing at 0.035 Hz was larger than that at 0.061 Hz, the associated energy density was smaller. Indeed, the larger cycle time at 0.035 Hz provided an opportunity for charges at the surface of the pyroelectric element to conduct through its body (leakage current) thus dissipating the energy as Joule heating. On the other hand, operating the device at a frequency larger than 0.061 Hz decreased the energy density of the pyroelectric material since the temperature swing was smaller as indicated in Fig. 11. Therefore, achieving the maximum energy density of the pyroelectric element was a compromise between

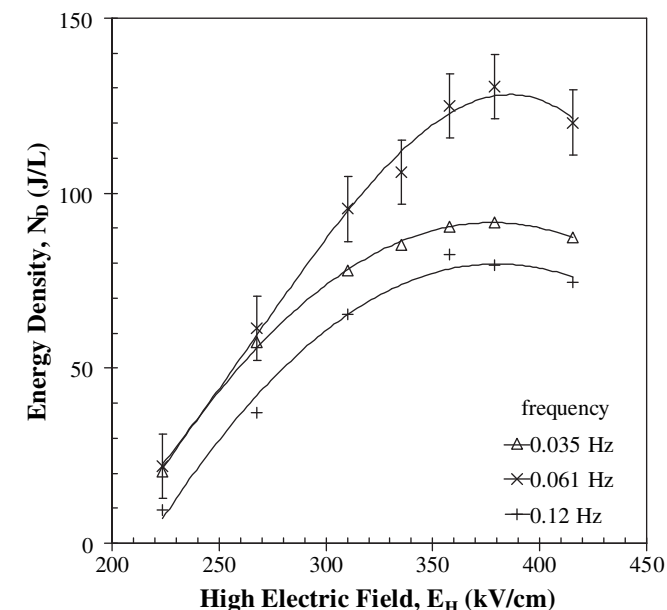


Fig. 12. Comparison of energy density for different frequencies as a function of high electric field  $E_H$ . The channel width, stroke length, low field, and mean temperature  $\bar{T}_3$  were constant and equal to 330  $\mu\text{m}$ , 4.7 cm, 202 kV/cm, and  $74 \pm 1 \text{ }^\circ\text{C}$ , respectively.

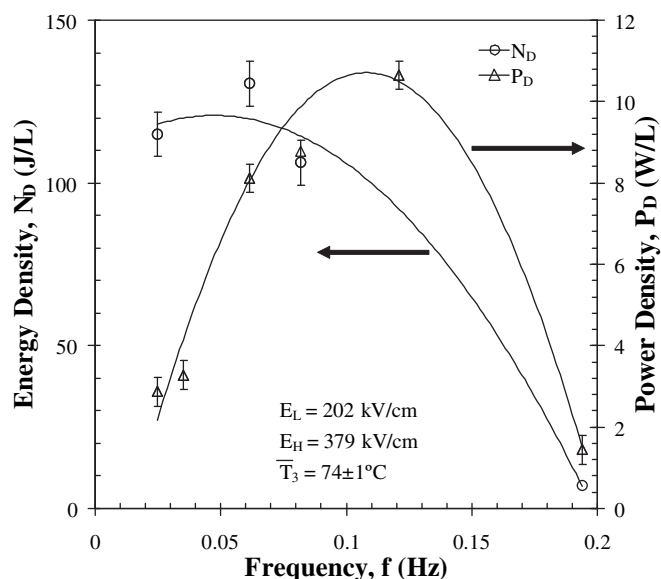


Fig. 13. Maximum energy and power densities as a function of frequency. The channel width, stroke length, and mean temperature  $\bar{T}_3$  were constant and equal to 330  $\mu\text{m}$ , 4.7 cm, and  $74 \pm 1 \text{ }^\circ\text{C}$ , respectively.

large temperature swing and small cycle time and leakage current. Fig. 13 also indicates that a maximum power density  $P_D$  of 10.7 W/l of pyroelectric material was obtained at 0.12 Hz. Although the energy density of the pyroelectric element was smaller at 0.12 Hz compared with 0.061 Hz, the fact that the cycle time was smaller resulted in a larger power density. Operating the device at frequency larger than 0.12 Hz, on the contrary, resulted in smaller power output due to a large reduction in output energy density caused by smaller temperature swing  $\Delta T_3$ .

#### 4.5. Heat losses to the surroundings

Efforts have been made to reduce the device heat losses to the surrounding by using Teflon for the device outer cylinders and fiberglass wool to entirely insulate the device. The device heat losses were estimated by performing an overall energy balance for the device. Heat losses were found to range from 15 to 20% of the total heat input  $\dot{Q}_{in}$  and increased as the operating temperature and heat input increased. For example, at 0.025 Hz, the heat input by the electrical heater was 26.6 W and the heat losses were 4.4 W. However, at 0.082 Hz, the heat input was 34.6 W and the heat losses were 6.7 W. In both cases, the stroke length,  $\bar{T}_3$ , and channel width were 4.7 cm,  $74 \pm 1 \text{ }^\circ\text{C}$ , 330  $\mu\text{m}$ , respectively. Because heat losses decrease the efficiency of the device, additional care must be taken to lower this parasitic losses. One solution is to use better insulating materials such as pyrogel whose thermal conductivity is half that of fiberglass wool [36].

#### 4.6. Efficiency

The device efficiency increased as the high electric field increased but reached a maximum at 379 kV/cm. The maximum efficiency for 0.061 and 0.12 Hz were 0.045% and 0.053%, respectively. Applying an electric field  $E_H$  smaller than 379 kV/cm decreased the power output and therefore the efficiency due to smaller field span and charge displacement. Moreover, applying an electric field  $E_H$  larger than 379 kV/cm decreased the efficiency due to larger current leakage through the PE. Note that the device was not optimized to achieve maximum efficiency but to maximize the energy and power densities per unit volume of PE. In particular, the efficiency was smaller than that reported by Olsen *et al.*[5] due to

(1) a smaller number of pyroelectric elements  $n_{PE}$  in the stack (38 compared to 100) and (2) smaller surface area of the pyroelectric element used for power generation.

## 5. Conclusion

This study was concerned with the design, assembly, and operation of a pyroelectric converter for harvesting waste heat by performing the Olsen cycle on 60/40 P(VDF-TrFE) thin films. First, the underlying physical principles were presented. Then, the pyroelectric device assembled and the associated thermal and electrical sub-systems were described in details. Finally, the experimental results were reported and discussed. The following conclusions can be drawn:

1. Temperature swing at the pyroelectric element decreased as frequency increased for constant arithmetic mean temperature at the center of the pyroelectric element  $\bar{T}_3$ .
2. The greatest increase in the device's energy and power densities was caused by reducing the channel width and increasing the piston stroke length.
3. For the same frequency, stroke length, and  $\bar{T}_3$ , the temperature swing  $\Delta T_3$  increased as the channel width decreased.
4.  $\Delta T_3$  also increased as stroke length increased. The optimum stroke length was theoretically determined to be 4.7 cm for the device assembled in this study.
5. In order to maximize the pyroelectric element energy and power densities, it was best to operate the device where the arithmetic mean temperature at center of the pyroelectric element  $\bar{T}_3$  was equal to  $74 \pm 1$  °C identified as the best compromise between large temperature swing and excessive leakage current.
6. Heat input required to maintain the mean temperature  $\bar{T}_3$  at  $74 \pm 1$  °C increased as stroke length and frequency increased.
7. The optimum high electric field  $E_H$  in the Olsen cycle was 379 kV/cm while  $E_L$  was set at 202 kV/cm.
8. The largest energy density achieved by the device was 130 J/l of pyroelectric material at 0.061 Hz while the largest power density was 10.7 W/l of pyroelectric material at 0.12 Hz. To the best of our knowledge, this is the largest energy density achieved by any pyroelectric energy converter using polymeric pyroelectric material P(VDF-TrFE).

Such a device could be used for waste heat recovery from internal combustion engines or various electronic devices. Future research should focus on (i) further reducing the channel width to increase the temperature swing and the number of pyroelectric elements in the stack to increase the device power density and the efficiency and on (ii) synthesizing inexpensive pyroelectric thin films with large surface area which feature large spontaneous polarization, electric breakdown field, and electrical resistivity at all operating temperatures.

## Acknowledgement

This study was supported by the University of California Energy Institute and the Office of Naval Research under Award N000140710671 (Program manager: Dr. Mark Spector). The authors would like to thank Dr. R.B. Olsen for useful discussions and exchange of information.

## References

- [1] Lawrence Livermore National Laboratory, U.S. energy flow trends. <http://eed.llnl.gov/flow> (2002) April 16, 2008.

- [2] S.B. Riffat, X. Ma, Thermoelectrics: a review of present and potential applications. *Applied Thermal Engineering* 23 (2003) 913–935.
- [3] B. Poudel, Q. Hao, Y. Ma, Y. Lan, A. Minnich, B. Yu, X. Yan, D. Wang, A. Muto, D. Vashaee, X. Chen, J. Liu, M.S. Dresselhaus, G. Chen, Z. Ren, High-thermoelectric performance of nanostructured bismuth antimony telluride bulk alloys. *Science* 320 (2008) 634–638.
- [4] B.T. Liu, K.H. Chien, C.C. Wang, Effect of working fluids on organic rankine cycle for waste heat recovery. *Energy* 29 (8) (2004) 1207–1217.
- [5] R.B. Olsen, D.A. Bruno, J.M. Briscoe, Cascaded pyroelectric energy converter. *Ferroelectrics* 59 (1984) 205–219.
- [6] R.B. Olsen, D.A. Bruno, J.M. Briscoe, Pyroelectric conversion cycles. *Journal of Applied Physics* 58 (1985) 4709–4716.
- [7] R.B. Olsen, D.A. Bruno, J.M. Briscoe, W.F. Butler, A pyroelectric energy converter which employs regeneration. *Ferroelectrics* 38 (1981) 975–978.
- [8] R.B. Olsen, Ferroelectric conversion of heat to electrical energy – a demonstration. *Journal of Energy* 6 (1982) 91–95.
- [9] R.B. Olsen, D.D. Brown, High-efficiency direct conversion of heat to electrical energy – related pyroelectric measurements. *Ferroelectrics* 40 (1982) 17–27.
- [10] R.B. Olsen, D.A. Bruno, J.M. Briscoe, Pyroelectric conversion cycle of vinylidene fluoride-trifluoroethylene copolymer. *Journal of Applied Physics* 57 (1985) 5036–5042.
- [11] S.B. Lang, Pyroelectricity: from ancient curiosity to modern imaging tool. *Physics Today* 58 (2005) 31–36.
- [12] J.N. Zemel, Future directions for thermal information sensors. *Sensors and Actuators A* 56 (1996) 57–62.
- [13] A. van der Ziel, Solar power generation with the pyroelectric effect. *Journal of Applied Physics* 45 (1974) 4128.
- [14] W.H. Clingman, R.G. Moore, Application of ferroelectricity to energy conversion processes. *Journal of Applied Physics* 32 (1961) 675–681.
- [15] M. Ikura, Conversion of low-grade heat to electricity using pyroelectric copolymer. *Ferroelectrics* 267 (2002) 403–408.
- [16] L. Kouchachvili, M. Ikura, High performance pyroelectric converter. In: *Proceedings of the Sixth IASTED International Conference European Power and Energy Systems*, Rhodes, Greece; 2006, pp. 366–371.
- [17] A. Khodayari, S. Pruvost, G. Sebald, D. Guyomar, S. Mohammadi, Nonlinear pyroelectric energy harvesting from relaxor single crystals. *IEEE Transactions on Ultrasonics, Ferroelectrics, and Frequency Control* 56 (2009) 693–699.
- [18] R.B. Olsen, J.M. Briscoe, Regenerative pyroelectric heat engine. In: *16th Intersociety Energy Conversion Engineering Conference*, Atlanta, Georgia; 1981, vol. 3, pp. 2081–2085.
- [19] M.A. Itskovsky, Pyroelectric hysteresis loop at ferroelectric phase transition. *Journal of Applied Physics* 85 (1999) 4256–4258.
- [20] S.B. Lang, D.K. Das-Gupta, in: *Handbook of Advanced Electronic and Photonic Materials and Devices*, vol. 4, Academic Press, San Diego, California, 2001.
- [21] H.M. Bao, J.F. Song, J. Zhang, Q.D. Shen, C.Z. Pang, Q.M. Zhang, Phase transitions and ferroelectric relaxor behavior in P(VDF-TrFE-CFE) terpolymers. *Macromolecules* 40 (2007) 2371–2379.
- [22] L. Kouchachvili, M. Ikura, Improving the efficiency of pyroelectric conversion. *International Journal of Energy Research* 32 (2008) 328–335.
- [23] L. Kouchachvili, M. Ikura, Pyroelectric conversion-effects of P(VDF-TrFE) preconditioning on power conversion. *Journal of Electrostatics* 65 (2006) 182–188.
- [24] K.J. Kim, G.B. Kim, C.L. Vanlencia, J.F. Rabolt, Curie transition, ferroelectric crystal structure and ferroelectricity of VDF/TrFE (75/25) copolymer: 1. The effect of the consecutive annealing in the ferroelectric state on curie transition and ferroelectric crystal structure. *Journal of Polymer Science* 32 (1994) 2435–2444.
- [25] R.B. Olsen, D.A. Bruno, Pyroelectric conversion materials. In *Proceedings of the 21st Intersociety Energy Conversion Engineering Conference*, American Chemical Society, Washington, D.C., 1986, pp. 89–93.
- [26] A. Navid, C.S. Lynch, L. Pilon, Purified and porous poly(vinylidene fluoride-trifluoroethylene) [P(VDF-TrFE)] thin films for pyroelectric infrared sensing and energy harvesting. *Smart Materials and Structures* 19 (2010) 055006.
- [27] V. Sencadas, S. Lanceros-Mendez, J.F. Mano, Characterization of poled and non-poled  $\beta$ -PVDF films using thermal analysis techniques. *Thermochimica Acta* 424 (2004) 201–207.
- [28] B. Chu, X. Zhou, K. Ren, B. Neese, M. Lin, Q. Wang, F. Bauer, Q.M. Zhang, A dielectric polymer with high electric energy density and fast discharge speed. *Science* 313 (2006) 334–336.
- [29] M.J. Moran, H.N. Shapiro, *Fundamentals of Engineering Thermodynamics*, fifth ed., John Wiley and Sons, New York, NY, 2004.
- [30] H.T. Nguyen, Pyroelectric energy converter using co-polymer P(VDF-TrFE) and Olsen cycle for waste heat energy harvesting. Master's thesis, University of California, Los Angeles. Department of Mechanical and Aerospace Engineering, 2010.
- [31] S.L. Kakani, A. Kakani, *Material Science*. New Age International Limited, New Delhi, India, 2004.
- [32] *Evolution Engines*. *Evolution Engines 26GT2/35GT2*, Doc. 7795.3 EVO. gas. manual.Final, 2009.
- [33] Dow Corning, Dow Corning 200 fluid, Ref. 22–0069N-01, 2009.
- [34] F.P. Incropera, D.P. DeWitt, *Heat and Mass Transfer*, fifth ed., John Wiley and Sons, New York, NY, 2002.
- [35] M. Ozawa, M. Shinoki, K. Nagoshi, E. Serizawa, Scaling of heat transfer characteristics in an oscillating flow. *Journal of Enhanced Heat Transfer* 10 (2003) 275–285.
- [36] Aspen Aerogels. Pyrogel XT, Ref. Pyrogel XT, 2009.